

Orbital phase resolved spectroscopy of GX 301-2 with MAXI

Nazma Islam^{1,2*} and Biswajit Paul¹

¹*Raman Research Institute, Sadashivnagar, Bangalore-560080, India*

²*Joint Astronomy Programme, Indian Institute of Science, Bangalore-560012, India*

ABSTRACT

GX 301-2, a bright HMXB with an orbital period of 41.5 days, exhibits stable periodic orbital intensity modulations with a strong pre-periastron X-ray flare. Several models have been proposed to explain the accretion at different orbital phases, invoking accretion via stellar wind, equatorial disk, and accretion stream from the companion star. We present results from exhaustive orbital phase resolved spectroscopic measurements of GX 301-2 using data from the Gas Slit Camera onboard *MAXI*. Using spectroscopic analysis of the *MAXI* data with unprecedented orbital coverage for many orbits continuously, we have found a strong orbital dependence of the absorption column density and equivalent width of the iron emission line. A very large equivalent width of the iron line along with a small value of the column density in the orbital phase range 0.10–0.30 after the periastron passage indicates presence of high density absorbing matter behind the neutron star in these orbital phase range. A low energy excess is also found in the spectrum at orbital phases around the pre-periastron X-ray flare. The orbital dependence of these parameters are then used to examine the various models about mode of accretion onto the neutron star in GX 301-2.

Key words: stars: neutron , stars: individual: GX 301-2 , X-rays: stars

1 INTRODUCTION

GX 301-2 is a High Mass X-ray Binary (HMXB) system with an X-ray pulsar and a B-emission line hypergiant star (B1 Ia+) WRAY 997. The orbital period of the binary system is ~ 41.5 days and the neutron star has a large spin period of ~ 685 s (Koh et al. 1997). The distance to GX 301-2 is estimated to be ~ 3.1 kpc (Coleiro & Chaty 2013). It is a highly eccentric binary system with $e=0.462$ (Sato et al. 1986; Koh et al. 1997) and has a periodically variable X-ray intensity.

The orbital characteristics of GX 301-2 have been extensively studied with various X-ray instruments in different energy bands (*CGRO-BATSE* (15–55 keV) - Koh et al. 1997) (*RXTE ASM* (2–12 keV) - Pravdo & Ghosh 2001; Leahy 2002; Leahy & Kostka 2008) (*SuperAGILE* (20–60 keV) - Evangelista et al. 2010). It has three intensity regimes: bright phase during X-ray flare (pre-periastron passage around orbital phase 0.95), dim or low intensity phase (after periastron passage around orbital phase 0.15–0.3) and intermediate intensity phase (during the apastron passage around orbital phase 0.5) (Koh et al. 1997; Leahy 2002). A strong X-ray flare occurs before the periastron passage as well as a medium intensity peak is observed at the apas-

tron passage, indicating accretion onto the neutron star due to both spherical stellar wind along with a possible equatorial disk or accretion stream (Sato et al. 1986; Stevens 1988; Haberl 1991; Layton et al. 1998; Pravdo & Ghosh 2001; Leahy & Kostka 2008).

The X-ray spectrum of GX 301-2 have been studied in different orbital phases with *TENMA* (Leahy & Matsuoka 1990), *ASCA* (Saraswat et al. 1996; Endo et al. 2002), *RXTE PCA* (Mukherjee & Paul 2004), *Chandra* (Watanabe et al. 2003), *BeppoSAX* (La Barbera et al. 2005), *XMM-Newton* (Fürst et al. 2011) and *Suzaku* (Suchy et al. 2012). It has a highly absorbed X-ray spectrum with a partial covering high energy cutoff power-law component and several emission lines. A soft excess component is found in the X-ray spectrum from *EXOSAT* and *ASCA* observations (Haberl 1991; Saraswat et al. 1996). GX 301-2 has a very high line of sight photo-electric absorption, which is attributed to the dense circumstellar environment in which the neutron star moves. The column density varies strongly with orbital phase with certain amount of clumpiness attributed to the stellar wind (Pravdo & Ghosh 2001; Mukherjee & Paul 2004; Leahy & Kostka 2008). A prominent Fe $K\alpha$ line is found to exist in almost all orbital phases of GX 301-2. This fluorescence line is produced due to reprocessing of X-ray photons from the pulsar by the circumstellar matter and sometimes shows evidence of a Compton recoil (Watanabe

* E-mail: nazma@rri.res.in;

et al. 2003).

The equivalent width of the Fe K α line depends on the distribution (geometry and column density) of the surrounding matter (Inoue 1985; Makino et al. 1985; Makishima 1986; Leahy & Creighton 1993; Kallman et al. 2004). Therefore, by comparing the equivalent width of Fe K α line with N_H , we can study the distribution of circumstellar matter around the neutron star at different orbital phases. This can be further used in examining the various accretion models of GX 301-2, in which the accretion rate and the reprocessing environment have strong orbital phase dependence. In this work, we have investigated the accretion phenomena in GX 301-2 using the orbital variation of column density of absorbing matter and the relation between the line equivalent width and N_H as observational parameters. For such studies, it is very useful to have long term orbital light-curves and spectrum measured at different orbital phases with uniform phase coverage. The Monitor of All Sky X-ray Image (*MAXI*), which has both all sky coverage and moderate energy resolution, is well suited for detailed studies of the orbital light-curves and the orbital phase resolved spectrum of bright X-ray sources.

In the present work, we have used light curves of GX 301-2 in the 2-20 keV energy range obtained over four years with the *MAXI-GSC* to create multi-band orbital intensity profiles. From spectroscopic analysis of the *MAXI* data with unprecedented orbital coverage for many orbits continuously, we have measured the orbital dependence of the absorption column density and equivalent width of the Fe K α line. The orbital phase dependence of the column density and the line equivalent width are then used to examine the various models about the distribution of circumstellar matter and the mode of accretion onto the neutron star in GX 301-2.

2 DATA AND ANALYSIS

2.1 Monitor of All Sky X-ray image

MAXI is an all sky monitor operated on the Kibo module of the International Space Station (ISS) (Matsuoka et al. 2009). It has the best sensitivity and energy resolution amongst all operating all sky monitors. It has two instruments onboard: Solid state Slit Camera (SSC), operating between 0.7-7 keV (Tomida et al. 2011) and Gas Slit Camera (GSC), operating in the energy range 2-20 keV (Mihara et al. 2011). We have used archival data from GSC¹ in this work. The GSC consists of six units of large area position sensitive Xenon proportional counters with an instantaneous field of view of $1.5^\circ \times 160^\circ$. It has 85% coverage of the entire sky in every 92 minutes of the ISS orbit. The typical daily exposure of GSC is 1500 cm²s. The in-orbit performance of GSC is summarised in Sugizaki et al. (2011).

2.2 Energy resolved orbital intensity profiles

We have first used 16 years long light-curve of GX 301-2 obtained with the *RXTE ASM* in 2-12 keV energy band (Levine et al. 1996) to estimate the orbital period of the system (P_{orb} =3584304 s; consistent with Koh et al. (1997)).

We have then folded the *MAXI-GSC* light curves of GX 301-2 obtained during MJD:55064 to 56502 with the orbital period obtained from *RXTE ASM* to obtain energy resolved orbital intensity profiles. The orbital phase reference is taken from Koh et al. (1997), with the phase zero corresponding to periastron passage. The orbital intensity profiles in the *MAXI* energy bands of 2-4 keV, 4-10 keV and 10-20 keV are shown in Figure. 1 along with hardness ratios (4-20 keV / 2-4 keV and 10-20 keV / 4-10 keV) of photons. The orbital modulation is most pronounced in the highest energy band of 10-20 keV showing the pre-periastron X-ray flare as well as the intermediate intensity apastron peak. In the lowest 2-4 keV energy band, instead of a strong flare, a sinusoidal modulation in intensity can be seen. This smoothly varying soft X-ray profile is seen for the first time in GX 301-2 with the *MAXI* data. As seen in Figure. 1, there is an increase in the 4-10 keV photons after the apastron passage, which is reflected in the low hardness ratio values around orbital phase 0.5-0.8.

2.3 Orbital phase averaged and phase resolved spectroscopy

2.3.1 Orbital phase averaged spectrum

We have extracted the orbital phase averaged spectrum of GX 301-2 with *MAXI GSC* for the same observation duration using the *MAXI* on-demand data processing². The orbital phase averaged spectrum is modelled with a power-law with a high energy cut-off modified by photoelectric absorption by column density of absorbing material along our line of sight. The spectral analysis is performed using *Xspec v:12.6*. Though the broadband X-ray spectrum of GX 301-2 is known to have a partial covering absorption (Mukherjee & Paul 2004; Suchy et al. 2012; La Barbera et al. 2005), in the limited energy band of the GSC, it was not required to include partial covering absorption in the spectral model. A Fe K α fluorescence line present in the spectrum is modelled with a single gaussian line. The analysis is carried out by fitting the spectrum from energy range 3.5 keV to 20 keV by a power-law with a high energy cut-off and a single gaussian line. When this fit was extended to lower energies till 2.0 keV, a low energy excess was found in the spectrum. This low energy excess was modelled by an unabsorbed blackbody component by freezing all other parameters of the previous best fit model. The motive behind modelling the low energy excess by an unabsorbed blackbody is to only estimate the flux of the low energy excess and not to derive a blackbody temperature and size of the region. The orbital phase averaged X-ray spectrum along with the best fit model components is shown in Figure. 2, along with the presence of soft excess, which is then modelled by a blackbody component. The χ^2_ν is 0.99 for 352 degrees of freedom.

2.3.2 Orbital phase resolved spectra

Strong variations of the hardness ratio of photons in 10-20 keV energy band and 4-10 keV energy band with

¹ <http://maxi.riken.jp/top>

² <http://maxi.riken.jp/mxondem/>

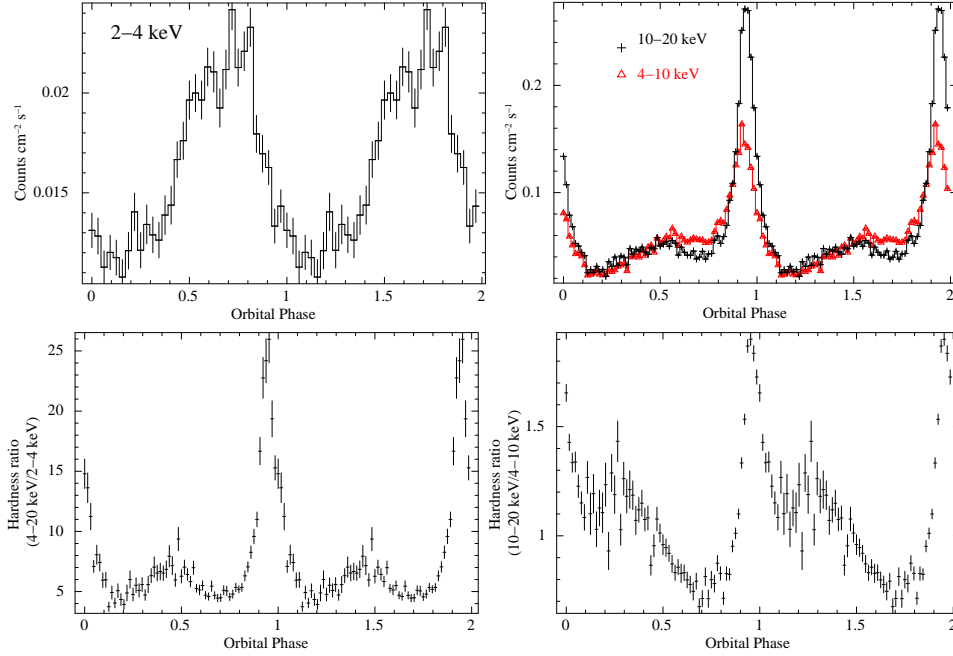


Figure 1. The top left panel is the orbital intensity profile of GX 301-2 in 2-4 keV energy band of MAXI. The top right panel is the orbital intensity profile in 4-10 keV (triangles) and 10-20 keV (cross) energy band. The bottom left panel is the hardness ratio (HR) of the counts in 4-20 keV energy band to low energy 2-4 keV band. Lower right panel is the hardness ratio of counts in 10-20 keV and 4-10 keV energy band.

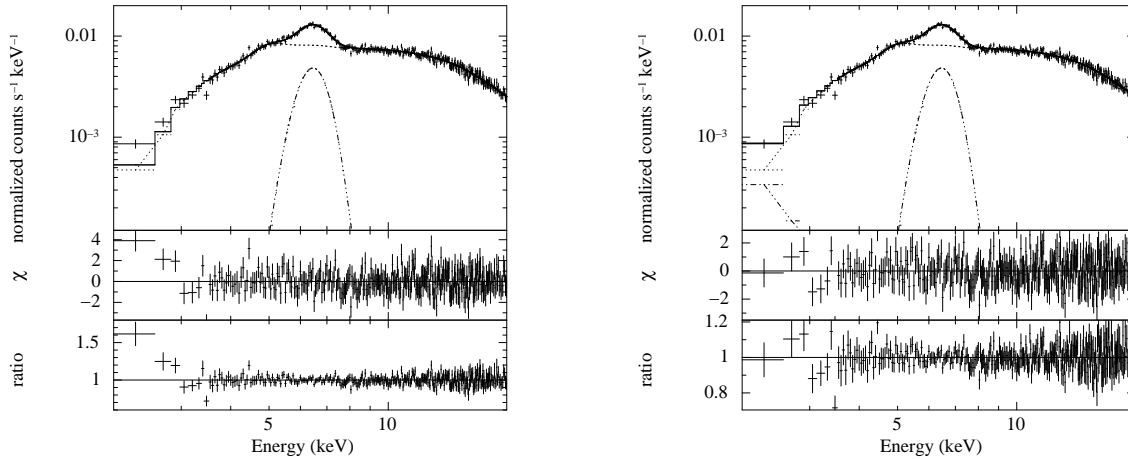


Figure 2. The orbital phase averaged X-ray spectrum is shown along with the best fit model components (top panel), contributions of the residuals to the chisquare (middle panel) and ratio between data and the model (bottom panel) in the 2-20 keV band. The best fit model is obtained in the energy range 3.5-20 keV and is extended to 2 keV. The left panel shows the presence of a soft excess and the right panel shows the fit after modelling the soft excess with a blackbody component.

the orbital phase shown in Figure. 1 indicates significant changes in the overall spectrum. Many observations of GX 301-2 have been carried out at different orbital phases in the past (Endo et al. 2002; Mukherjee & Paul 2004; La Barbera et al. 2005; Suchy et al. 2012), but with uneven phase coverage. We have performed an orbital phase resolved spectral analysis of GX 301-2, by using the arbitrary grouping of the individual scans allowed by MAXI on demand data processing (Nakahira et al. 2012; Doroshenko et al. 2013). Using the orbital ephemeris, we extracted the start time and end time for different orbital

phase bins, and extracted the spectra for each orbital phase with data from multiple orbital cycles by grouping the individual scans. We have chosen 21 independent orbital bins, with the bin size chosen such that it can constrain the Fe line parameters. The effective exposure times varies from 43 kilosec for the orbital bins near the X-ray peak to 454 kilosec for orbital bins near dim phase. In this work, we have fitted these 21 orbital phase resolved spectra with two models: a power-law continuum, with and without a high energy cut-off. For the spectral fits with a high energy cut-off, the value of cut-off energy and fold

energy (E_c and E_f) was frozen to the orbital phase averaged values of 15 keV and 18.6 keV respectively, since the parameters of the high energy cut-off cannot be constrained well in the phase resolved spectra. A Fe fluorescence line was found in all the orbital phases which was modelled by a single gaussian line. For both the spectral models, the spectra were fitted from energy range 3.5 keV to 20 keV and then the fit was extended to lower energies till 2.0 keV. For some orbital phases near the X-ray peak, a low energy excess is found to be present in the spectra. To only estimate the flux in the soft excess, we have modelled the low energy excess with an unabsorbed blackbody component. The range of χ^2_ν values, after accounting for the low energy excess), is 0.8-1.16 (0.75-1.23) for a power-law with high energy cut-off (without the high energy cut-off).

The orbital dependance of the spectral parameters photon index Γ , column density of absorbing matter along our line of sight N_H , flux and equivalent width of Fe line emission, total flux of the system in the entire 2-20 keV energy band of *MAXI GSC* and ratio of flux included in the low excess to the total flux of the system, for both the spectral models are shown in the Figure. 3. The errors on the spectral parameters Γ , N_H and flux of Fe line emission are at 90% confidence level whereas the errors on equivalent width of Fe line is shown at 1σ confidence level. The errors on the relative flux in the low energy excess, modelled by a blackbody is taken at 1σ confidence level of blackbody normalisation. Since the high energy cut-off affects the X-ray spectrum only above 15 keV, therefore the two results shown in Figure. 3 with and without the high energy cut-off included in the spectral model show similar pattern of variation of the spectral parameters.

The orbital variation of column density of absorbing matter along our line of sight N_H and flux of Fe line emission for both the spectral models follows the orbital variation of the flux of the system. However, orbital variation of power-law photon index and equivalent width of Fe line follows a different pattern from the flux of the system. The power-law photon index Γ is hard at the dim phase and at the pre-periastron X-ray flare and is soft around the apastron passage. The orbital variation of equivalent width has two peaks and the lowest equivalent width occurs at the apastron passage. The soft excess is detected only near the X-ray flare and has a flux that is less than 1.0% of the continuum flux.

Three of the phase resolved X-ray spectra showing the highest equivalent width of Fe line (dim phase : 0.1-0.2), lowest equivalent width (intermediate phase: 0.475-0.55) and at pre-periastron flare (phase 0.95) are shown in Figure. 4.

3 DISCUSSIONS

3.1 Multi-band orbital modulation

Figure. 1 shows the orbital intensity profiles of GX 301-2 in 2-4 keV, 4-10 keV and 10-20 keV energy bands of *MAXI*, along with the hardness ratios of photons in 4-20 keV energy band to 2-4 keV energy band and 10-20 keV energy band to 4-10 keV energy band. We have detected a strong,

nearly sinusoidal, modulation by a factor of ~ 2.5 in the 2-4 keV energy band, the profile of which is different from the orbital modulation in the 4-20 keV band. In the entire 4-20 keV band and other sub-bands (4-10 keV and 10-20 keV), the source shows an appreciable orbital modulation, as previously known, with a strong pre-periastron X-ray flare as well as an apastron peak. The hardness ratio between the 10-20 and 4-10 keV bands shows the pre-periastron X-ray flare to be hard which is also reflected in small value of the power-law photon index at the phase ~ 0.95 (Figure. 3). After the apastron passage and before the hard X-ray flare (orbital phase range 0.55-0.85), there is a decrease seen in the hardness ratio. A corresponding high value of the power-law photon index Γ is seen in the Figure. 3.

3.2 Variation of Spectral parameters with Orbital Phase

We have studied the orbital dependence of different spectral parameters of GX 301-2 using a power-law continuum model with and without a high energy cut-off. Figure. 3 shows the orbital variation of Γ , N_H , flux and equivalent width of Fe fluorescence line, total flux of the system and ratio of flux included in the low excess to the total flux, for both the spectral models. From Figure. 3, the orbital variation in spectral parameters for both the models show very similar trend. The photon index gradually increases from a low value of 0.05 for power-law with high energy cut-off (0.3 for power-law) model at the dim orbital phase 0.1-0.3, to 1.1 for both the models at the periastron passage, just before the X-ray flare. The spectrum is found to be hard at dim phase 0.1-0.3 for both the models. Spectral hardening at this phase was reported in earlier works using data from *RXTE-ASM* and *SuperAGILE* (Pravdo & Ghosh 2001; Evangelista et al. 2010).

The column density N_H is found to vary with a pattern similar to the flux of the system, indicating a possible origin of flare due to increased mass accretion at the orbital phase of ~ 0.95 . The absorption column density is in the range of $10\text{--}20 \times 10^{22} \text{ cm}^{-2}$ during most of the orbit, except near the flare. Since the data from *MAXI* is averaged over multiple orbital cycles, clumpiness in wind as seen in *RXTE PCA* data over one cycle (Mukherjee & Paul 2004) and *BepoSAX* data over one cycle (La Barbera et al. 2005), is not detectable in the *MAXI* data and a partial covering absorption is not required to fit the X-ray spectra obtained with *MAXI GSC*. The flux of Fe line emission also shows a strong increase during the flare, by a factor of ~ 3 , compared to the nearly constant flux in the orbital phase range 0.1-0.8. The orbital variation of equivalent width of Fe line shows a markedly different trend as compared to the orbital variation of column density and total flux of the system. The highest equivalent width occurs at the dim phase of 0.1-0.3 which also has lowest N_H along the line of sight. This different pattern of orbital variation of equivalent width and the column density N_H provides us important clues about the distribution of matter around the system, which is discussed further in the next section.

A low energy excess, contributing to less than 1.0% of the continuum flux, is found in the spectra at orbital phases near the pre-periastron X-ray flare as shown in the bottom panels of Figure. 3. Low energy excesses in the X-ray spectrum of

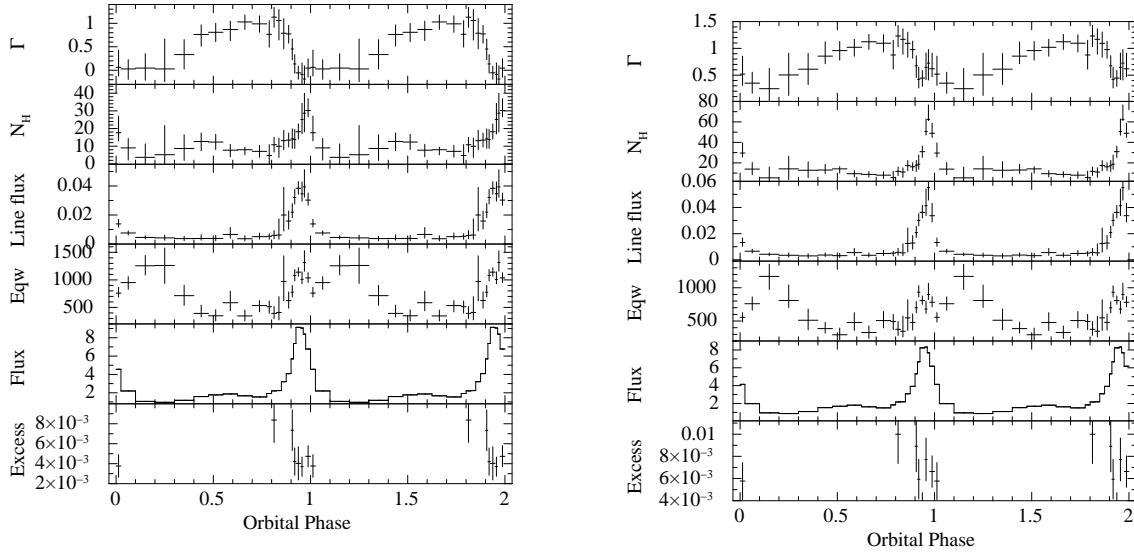


Figure 3. Variation of Photon index (Γ), equivalent column density of hydrogen (N_H in units of 10^{22} cm^{-2}), Line flux of Fe $K\alpha$ (in units of photons $\text{cm}^{-2} \text{ s}^{-1}$), Equivalent width of Fe $K\alpha$ line (Eqw in units of eV), Flux of source (F in the units of $10^{-9} \text{ ergs s}^{-1} \text{ cm}^{-2}$) and the ratio of flux in the low energy excess modelled by a blackbody to the flux of the system (Excess) for both the spectral models: power-law with a high energy cut-off (left panel) and a power-law (right panel).

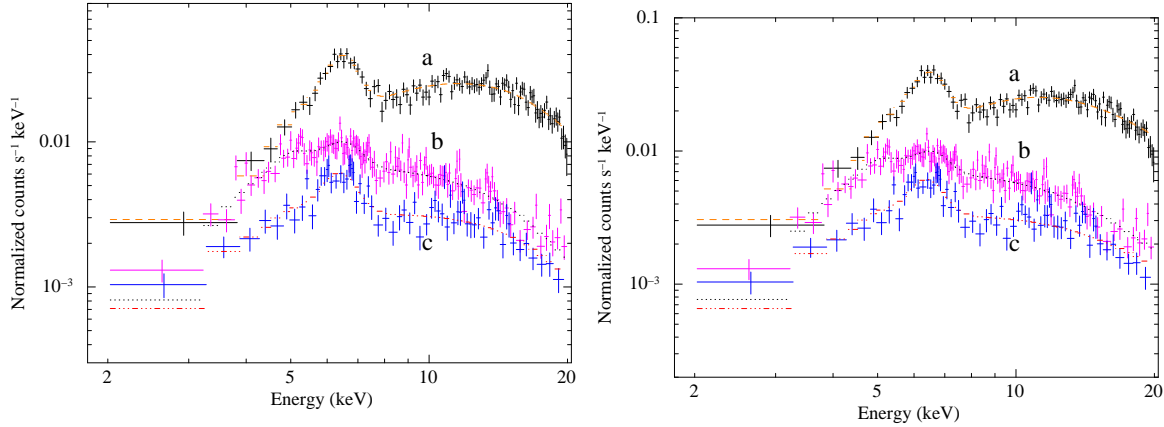


Figure 4. The spectra and the best fitted model are shown here for three different orbital phases: the pre-periastron X-ray flare (a), the apastron passage which has the lowest equivalent width of the iron line (b) and the dim phase which has the highest width of the iron line (c), for both the spectral models, i.e power-law with a high energy cut-off (left panel) and power-law model (right panel).

GX 301-2 has been previously reported by Haberl (1991) using *EXOSAT* observation and Saraswat et al. (1996) using *ASCA* observation. Due to high value of N_H around the X-ray flare, we rule out the possible origin of low energy excess from the surface of the neutron star (Hickox et al. 2004). A possible origin of this low energy excess could be due to the X-ray shocks in the system when the high density accretion stream interacts with the stellar wind from WRAY 977 (Haberl 1991; Kaper et al. 2006).

3.3 Orbital modulation: wind diagnostics

3.3.1 Column density as tracer

Figure. 5 shows the orbital variation of the column density of absorbing matter along our line of sight N_H obtained in this work with *MAXI* for both a power-law with a high energy cut-off model and a power-law model and is com-

pared to the predicted orbital variation of N_H expected from Pravdo & Ghosh (2001) and Leahy & Kostka (2008) models. These models were developed to describe the orbital intensity profile of GX 301-2 as seen with *BATSE* (Pravdo & Ghosh 2001) and *RXTE ASM* (Leahy & Kostka 2008). For the sake of comparison with the measured orbital profile of the column density, we have normalised the highest column density predicted by these models to the highest observed column density.

The Pravdo & Ghosh (2001) model predicts an enhanced column density twice, at the pre-periastron X-ray flare and at the dim orbital phase. However, only one peak in column density is observed with *MAXI* during pre-periastron passage. The Leahy & Kostka (2008) model underestimates the value of column density at the pre-periastron phase but predicts a large increase in column density around phase 0.2. On the other hand, the *MAXI GSC* spectra do not show an enhanced column density at orbital phase 0.1-0.3 predicted

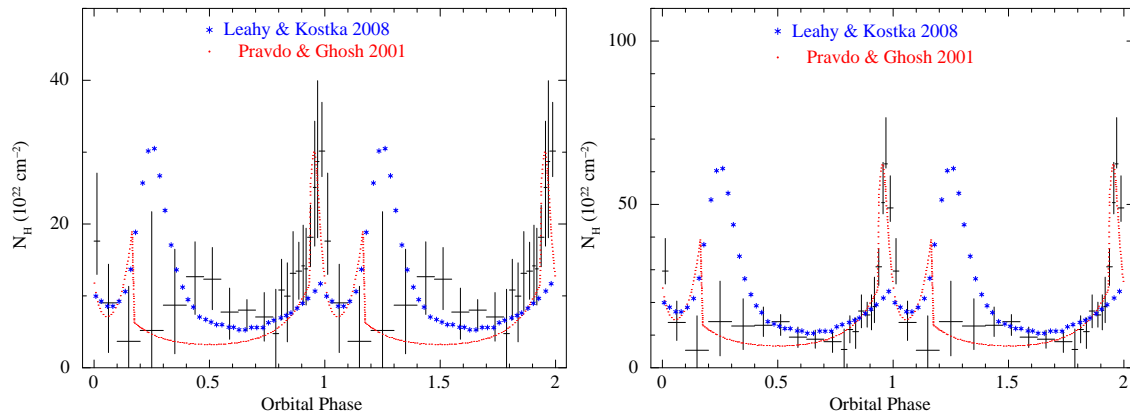


Figure 5. Variation of column density N_H as function of orbital phase of GX 301-2 for both power-law with high energy cut-off (left panel) and power-law model (right panel), overlaid on the predicted orbital variation of column density (circles - Pravdo & Ghosh (2001), asterisks - Leahy & Kostka (2008)). The predicted orbital variation of column density is normalised to the highest column density found in our results for the sake of comparing with the observed orbital profile.

by both the models, in our results. A possible explanation for this would be that the absorbing matter considered in these two models is situated away from the line of sight at this phase range. To further investigate this possibility, we have used the orbital variation of the equivalent width of the fluorescent iron line in the next section as an additional observational signature to study the orbital distribution of circumstellar matter around the neutron star in GX 301-2.

3.3.2 Iron line as tracer

The iron fluorescence line provides important information on the geometry and density of the line producing region around the central X-ray source that produces the continuum X-ray emission (Makishima 1986). In HMXBs, the fluorescence lines originate from the dense absorbing material present in the stellar wind. The detection of a Compton shoulder of Fe $K\alpha$ in GX 301-2 by Watanabe et al. (2003) confirms the presence of Compton thick matter around the X-ray source. The equivalent width of the Fe line is expected to be linearly correlated to the column density for an isotropically distributed cold matter (Inoue 1985; Kallman et al. 2004). Deviation from this linear correlation can be mostly attributed to any anisotropic configuration of the reprocessing matter around the X-ray source.

Figure. 6 shows the plot of equivalent width of the iron line against the absorbing column density N_H in different orbital bins for GX 301-2 in this work for both the spectral models. In certain orbital phases, we do see very high equivalent width (~ 1 keV) along with a small value of column density ($\sim 2-5 \times 10^{22} \text{ cm}^{-2}$). These observations highly deviate from the relation expected for an isotropically distributed gas (Inoue 1985; Kallman et al. 2004) and instead there seems to exist high anisotropy in the distribution of circumstellar matter around the X-ray pulsar, especially in some orbital phases. Our results are in contrast to the studies by Makino et al. (1985); Endo et al. (2002); Fürst et al. (2011), where they found a linear correlation between equivalent width and column density, thereby favouring a spherical shell model of gas distribution. However, such studies were carried out in narrow window of pointed observations

and this work is carried by averaging over multiple orbital cycles.

From orbital variation of N_H and equivalent width shown in Figure. (3), we see a very high equivalent width for very low line of sight column density at orbital phases 0.1-0.3. This being an important outcome of the present work and the fact that it is hardest to measure absorption column density in the dim phase, we have further examined it. As the MAXI-GSC spectrum has very little count-rate below 3 keV, we carried out the spectral analysis above 3.5 keV and an upper limit on N_H of $11 \times 10^{22} \text{ cm}^{-2}$ is obtained at the orbital phase 0.1-0.3 with a 90% confidence limit. Near the flare phase, the spectrum has higher statistics and the best fit model for the spectrum above 3.5 keV, when extended to the lower energy band, clearly shows the presence of a soft excess. The blackbody temperature of the soft excess measured in these phases is in the range of 0.1-0.3 keV and this component does not have any significant contribution in the GSC spectrum above 3.5 keV. Therefore, the value of N_H measured at different orbital phases (especially at dim phase of 0.1-0.3) represents the true line of sight value of N_H . A possible explanation would be that the distribution of circumstellar matter in these orbital phases somehow avoids the line of sight and the possible geometries could be the ones in which the reprocessing region (where the Fe fluorescence line is produced) is situated behind the neutron star or on one side of the neutron star away from the line of sight. The optical studies of GX 301-2 done by Kaper et al. (2006) confirms the presence of gas stream trailing the X-ray pulsar around the orbital phases 0.18-0.34. This would also be a possible explanation for the absence of second peak in the orbital distribution of N_H , though it is predicted both by Pravdo & Ghosh (2001) and Leahy & Kostka (2008) models.

4 SUMMARY

We have investigated the long term orbital variation of spectral parameters by exhaustive orbital phase resolved spectroscopic measurements of GX 301-2 with *MAXI*. The column density and flux of the Fe fluorescence line has a large value

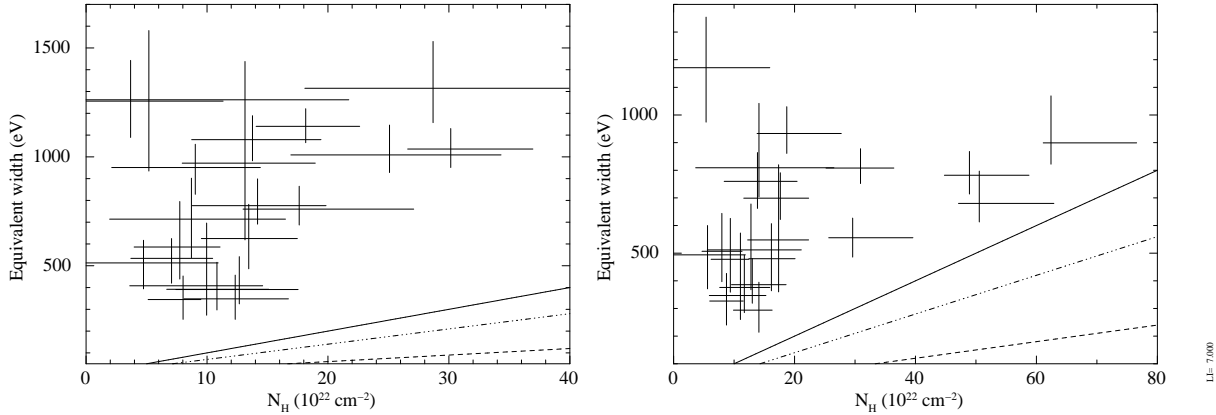


Figure 6. Plot of equivalent width of Fe K α versus absorbing column density N_H obtained for different orbital phases with MAXI for both power-law with highcut (left panel) and power-law model (right panel). Solid line represents the relation between equivalent width and column density of absorbing matter for isotropically distributed matter for $\Gamma \sim 1.1$ calculated by Inoue (1985). The dashed line and dot dashed line is the relation between equivalent width and column density for a spherical shell of gas for $\Gamma \sim 1$ and $\Gamma \sim 0.2$ respectively calculated by Kallman et al. (2004). $\Gamma \sim 0.2$ corresponds to the hardest spectrum seen in the dim phase with MAXI, where the highest value of equivalent width is found.

around the pre-periastron passage, suggesting the possible origin of X-ray flare due to enhanced mass accretion. A large column density and strong Fe emission line together with the presence of low energy excess in orbital phases around the X-ray flare, strongly favours a high density gas stream plus a stellar wind model for mode of accretion onto the neutron star in GX 301-2 (Leahy & Kostka 2008). The orbital dependence of column density and equivalent width of Fe line presented in this work provides stronger constraints to the dynamical wind plus stream model of Leahy & Kostka (2008). The presence of very high equivalent width of Fe line for very low column density along line of sight at orbital phases 0.1-0.3 places constraints on the direction of gas stream around GX 301-2 orbit. This has deep implications in understanding the interplay of accretion stream and stellar wind at different orbital phases. The relation between equivalent width of Fe line and column density of absorbing matter is a powerful tool which can be later used for probing the geometry and distribution of circumstellar matter around other wind-fed systems.

ACKNOWLEDGMENT

The authors are deeply grateful to Dr. T. Mihara for his helpful comments and suggestions. The authors also thank the anonymous referee for useful comments. This research has made use of MAXI data provided by RIKEN, JAXA and the MAXI team. This research has also made use of quick-look results of RXTE-ASM obtained through High Energy Astrophysics Science Archive Research Center Online Service (HEASARC), provided by the NASA/Goddard Space Flight Center.

REFERENCES

- Coleiro, A., & Chaty, S. 2013, ApJ, 764, 185
- Doroshenko, V., Santangelo, A., Nakahira, S., et al. 2013, A&A, 554, A37
- Endo, T., Ishida, M., Masai, K., et al. 2002, ApJ, 574, 879
- Evangelista, Y., Feroci, M., Costa, E., et al. 2010, ApJ, 708, 1663
- Fürst, F., Suchy, S., Kreykenbohm, I., et al. 2011, A&A, 535, A9
- Haberl, F. 1991, ApJ, 376, 245
- Hickox, R. C., Narayan, R., & Kallman, T. R. 2004, ApJ, 614, 881
- Inoue, H. 1985, Space Sci. Rev., 40, 317
- Kallman, T. R., Palmeri, P., Bautista, M. A., Mendoza, C., & Krolik, J. H. 2004, ApJS, 155, 675
- Kaper, L., van der Meer, A., & Najarro, F. 2006, A&A, 457, 595
- Koh, D. T., Bildsten, L., Chakrabarty, D., et al. 1997, ApJ, 479, 933
- La Barbera, A., Segreto, A., Santangelo, A., Kreykenbohm, I., & Orlandini, M. 2005, A&A, 438, 617
- Layton, J. T., Blondin, J. M., Owen, M. P., & Stevens, I. R. 1998, New A, 3, 111
- Leahy, D. A. 2002, A&A, 391, 219
- Leahy, D. A., & Creighton, J. 1993, MNRAS, 263, 314
- Leahy, D. A., & Kostka, M. 2008, MNRAS, 384, 747
- Leahy, D. A., & Matsuoka, M. 1990, ApJ, 355, 627
- Levine, A. M., Bradt, H., Cui, W., et al. 1996, ApJ, 469, L33
- Makino, F., Leahy, D. A., & Kawai, N. 1985, Space Sci. Rev., 40, 421
- Makishima, K. 1986, The Physics of Accretion onto Compact Objects, 266, 249
- Matsuoka, M., Kawasaki, K., Ueno, S., et al. 2009, PASJ, 61, 999
- Mihara, T., Nakajima, M., Sugizaki, M., et al. 2011, PASJ, 63, 623
- Mukherjee, U., & Paul, B. 2004, A&A, 427, 567
- Nakahira, S., Koyama, S., Ueda, Y., et al. 2012, PASJ, 64, 13
- Pravdo, S. H., & Ghosh, P. 2001, ApJ, 554, 383
- Saraswat, P., Yoshida, A., Mihara, T., et al. 1996, ApJ,

463, 726

Sato, N., Nagase, F., Kawai, N., et al. 1986, ApJ, 304, 241

Stevens, I. R. 1988, MNRAS, 232, 199

Suchy, S., Fürst, F., Pottschmidt, K., et al. 2012, ApJ, 745, 124

Sugizaki, M., Mihara, T., Serino, M., et al. 2011, PASJ, 63, 635

Tomida, H., Tsunemi, H., Kimura, M., et al. 2011, PASJ, 63, 397

Watanabe, S., Sako, M., Ishida, M., et al. 2003, ApJ, 597, L37